This is an Accepted Manuscript for *Journal of Glaciology*. Subject to change during the editing and production process.
DOI: 10.1017/jog.2024.20

Evolution of sub-ice-shelf channels reveals changes in ocean-driven melt in West Antarctica

Karen E. Alley[1], Richard B. Alley[2], Alex D. Crawford[1], Naomi Ochwat[3], Christian T. Wild[4], Juliana Marson[1], Tasha Snow[5], Atsuhiro Muto[6], Erin C. Pettit[7], Sarah Child[3], Martin Truffer[8], Gabi Collao-Barrios[3], Ted Scambos[3]

[1] Department of Environment and Geography, University of Manitoba, Winnipeg, MB, CAN
[2] Department of Geosciences, Pennsylvania State University, State College, PA, USA
[3] Cooperative Institute for Research in Environmental Sciences, University of Colorado Boulder, Boulder CO, USA
[4] Department of Geosciences, University of Tübingen, Tübingen, Germany
[5] Department of Geophysics, Colorado School of Mines, Golden, CO, USA
[6] Department of Earth and Environmental Science, Temple University, Philadelphia, PA, USA
[7] College of Earth, Ocean, and Atmospheric Sciences, Oregon State University, Corvallis, OR, USA
[8] Department of Physics, University of Alaska Fairbanks, Fairbanks, AK, USA

ABSTRACT

Basal channels, which are troughs carved into the undersides of ice shelves by buoyant plumes of water, are modulators of ice-shelf basal melt and structural stability. In this study, we track the evolution of 12 large basal channels beneath ice shelves of the Amundsen and Bellingshausen Seas region in West Antarctica using the Landsat record since its start in the 1970s through 2020. We observe examples of channel growth, interactions with ice-shelf features, and systematic changes in sinuosity that give insight into the life cycles of basal channels. We use the last two decades of the record, combined with contemporary ice-flow velocity datasets, to separate channel path evolution into components related to advection by ice flow and those controlled by other forcings, such as ocean melt or surface accumulation. Our results show that ice-flow-independent lateral channel migration is overwhelmingly to the left when viewed down-flow, suggesting that it is dominated by Coriolis-influenced ocean melt. By applying a model of channel-path evolution dominantly controlled by ice flow and ocean melt, we show that the majority of channels surveyed exhibit non-steady behavior that serves as a novel proxy for increased ocean forcing in West Antarctica starting at least in the early 1970s.

INTRODUCTION

Much of the sector of the West Antarctic Ice Sheet centered on the Amundsen and Bellingshausen Seas region (ABS) is experiencing sustained rapid ice-mass loss and

grounding-zone retreat (e.g. Lee and others, 2012; Smith and others, 2020) in direct response to ocean forcing (e.g. Pritchard and others, 2012; Alley and others, 2014; Scambos and others, 2017). These changes are driven primarily by the presence of warm modified Circumpolar Deep Water (mCDW), which crosses the continental shelf through troughs carved during repeated past glacial maxima (e.g. Jacobs and others, 2012; Nakayama and others, 2018; Morlighem and others, 2020). mCDW has increasingly accessed deep grounding zones and forced changes in floating ice shelves in the ABS in recent decades (e.g. Jacobs and others, 2012; Scambos and others, 2017). Many of these ice shelves play a pivotal role in stabilizing grounded ice through "backstress" that is transmitted upstream from contact with shallow sections of the seafloor or embayment walls (e.g. Dupont and Alley, 2005). Loss of this backstress due to ice-shelf weakening or disintegration leads to acceleration of upstream ice and greater contributions to global sea-level rise (e.g. Fürst and others, 2016; Gudmundsson and others, 2019); for example, recent accelerations at Pine Island Glacier, one of the largest outlet glaciers in West Antarctica, can be largely attributed to thinning and calving of the floating ice shelf (Joughin and others, 2021, De Rydt and others, 2021).

mCDW also likely forces the formation of basal channels (Alley and others, 2016), which are features that form on the undersides of ice shelves where buoyant meltwater plumes driven by ocean-induced melt (Rignot and Steffen, 2008; Gladish and others, 2012; Dutrieux and others, 2013; Alley and others, 2016; Gourmelen and others, 2017) and/or channelized subglacial discharge (Le Brocq and others, 2013; Marsh and others, 2016; Drews and others, 2017) carve troughs in the ice-shelf base. While small channels can be fully supported by bridging stresses (Langley and others, 2014; Drews, 2015), large basal channels are visible in optical satellite imagery as the overlying ice shelf hydrostatically adjusts to the thinner ice along channels. Most large channels are found beneath the warm-based ice shelves of the ABS (Alley and others, 2016). Basal channels impact ice-shelf stability in many ways. They modify basal-melt patterns, at least initially focusing melt within channel troughs (Millgate and others, 2013; Gourmelen and others, 2017) or redistributing melt to the keels between channels in outer ice-shelf areas (Dutrieux and others, 2013). Basal channels can also influence surface hydrology (Bell and others, 2017; Dow and others, 2018, Macdonald and others, 2018), and structurally weaken ice shelves, often along already-weakened shear margins (Dow and others, 2018; Alley and others, 2019, 2023; Wang and others, 2023).

Because basal channels impact ice-shelf stability through structural weakening, predicting ice-shelf evolution requires an understanding of basal channel change over time. Furthermore, since basal channels are products of ice-ocean interaction, basal channel changes can provide clues to ocean changes happening beneath ice shelves, as well as the ice-dynamic processes shaping them on the surface. Limited multi-annual time-series analyses have been carried out on a few individual basal channels. These studies suggest that channels can change significantly on interannual to decadal timescales. For example, Marsh and others (2016) showed high basal melt rates and rapid deepening in a subglacially sourced basal channel near the grounding zone of the Ross Ice Shelf using altimetry from the ICESat period. Alley and others (2016) observed similar, very rapid deepening in an ocean-sourced channel on the Getz Ice Shelf during the ICESat record, along with approximately 20 km of headward (upstream)

https://doi.org/10.1017/jog.2024.20 Published online by Cambridge University Press

growth over several decades of Landsat imagery. Chartrand and Howat (2020) confirmed continued deepening on the same Getz channel and noted subtle lateral migration to the left when facing downstream. Drews and others (2020) observed lateral migration of a basal channel on the Roi Baudouin Ice Shelf, which they attributed primarily to wind-driven deposition and erosion of surface snow.

In this study, we seek to better understand the evolution of basal channels, and of the ocean and ice-dynamic forcings that control them, by evaluating horizontal channel path changes observed at 12 large basal channels in the ABS throughout the Landsat record. For each channel, we track several decades of path change, sinuosity trends, and interactions with ice-shelf flow and structural features, which reveal information about the growth and life cycles of basal channels. Our results show non-steady behavior throughout the record, along with strong evidence of oceanic control on channel evolution. When interpreted using a conceptual model of channel-path evolution controlled by ocean melt and ice-shelf flow, these results suggest that basal channels have recorded evidence of changing ocean forcing in some parts of the ABS dating back to at least the early 1970s.

METHODS

Channel path time series

This study tracks the plan-view evolution of 12 basal channels in the ABS using a time series of Landsat imagery (Figure 1). All ocean-sourced channels identified by Alley and others (2016) were initially considered. Ocean-sourced channels are those that originate downstream of the grounding line, and are therefore assumed to be formed by ocean-driven plumes rather than subglacial discharge (Alley and others, 2016), although it is possible that the plumes are influenced directly or indirectly by subglacial discharge (Wei and others, 2020). Of these channels, we selected those that are >25 km long, clearly visible throughout the imagery record, and unconfined by a shear margin along at least 80% of their length. We also limited our analysis to channels that persist to the calving front, indicating that melting within the channel is vigorous enough to maintain the channel to the ice edge. These criteria were imposed to ensure that the channels analyzed were comparable in size and origin, that they could freely experience lateral migration without the influence of topographic barriers, and that they were likely actively shaped by ocean plume processes throughout the record. While there is no reason to suggest that the physics discussed in this manuscript are different for smaller channels or those that do not reach the ice edge, this subset was selected as the most likely to yield a high signal-to-noise ratio when investigating controls on channel paths.

Time series of each channel path (Supplemental Figure 1) were developed using imagery from Landsat 1-3 (band 6, 30 m resolution, 1972-1982), Landsat 4-5 (band 3, 30 m resolution, 1982-1999), and Landsat 7-8 (panchromatic band 8, 15 m resolution, 1999-2020), with one image per summer season for as many years as are available. Images from Landsat 1-5 were georeferenced to a recent Landsat-8 image using rock outcrops and non-moving features on grounded ice as tie points. Images with clouds covering a portion of the channel or with surface meltwater that obscured channel traces were excluded from the analysis.

https://doi.org/10.1017/jog.2024.20 Published online by Cambridge University Press

Each of the 12 channels was manually digitized by tracing the channel centerline on the selected Landsat images. Tributaries of the main channels were excluded from the analysis. Digitization was performed with images in a random order, and each profile was digitized with no other profiles visible. Every time series was digitized twice by two investigators working independently. All repeat digitizations yielded consistent results in migration direction and sinuosity change. Discrepancies in digitizations result from random error, systematic error due to, for example, differences in interpretation of shadows, and selection of different branches of the same channel. The latter error was addressed by limiting migration comparisons to within records developed by the same investigators. Random errors were addressed by calculating the root-mean-square distance between the channel traces digitized by the two investigators. When systematic error was clearly present (i.e., the shift between channel paths from each investigator was always in the same direction), the mean distance between traces was subtracted before calculating root-mean-square distance. This random error was added as a buffer on both sides of channel traces and is shown in both main-text and supplementary figures.

Quantifying lateral channel movement

The digitizations through time showed that, for most of the channels, traced paths are spread out, allowing for the quantification of lateral movement in channel paths. This lateral movement in channel paths is difficult to analyze for channels that exhibit persistent meandering behavior (Venable 1, Abbot, Getz 1), as the radius of the meanders is larger than any clear lateral migration, and therefore the downstream advection of meanders over time obscures any lateral movement trends. We exclude these three meandering channels from our quantitative analysis of lateral channel migration. We also exclude Stange 1 from this analysis. The ocean plumes that drive most basal channels flow in approximately the same direction as ice flow, as they follow the ice-base gradient. As discussed in detail later, our conceptual model of channel path movement relies on the ice and ocean plume flowing in approximately the same direction. However, based on observations of a persistent polynya at the end of the channel (Supplementary Fig. 1), which indicates the direction of ocean flow within the channel (following similar analyses by Bindschadler and others 2011, Mankoff and other 2012, Alley and others 2016, and Alley and others 2019) Stange 1 appears to experience plume flow and ice flow in opposite directions. Since we would expect this to result in behavior distinct from all of the other channels in the study, its comparison in this analysis is prevented.

For the remaining eight channels, we can quantify lateral movement of channel traces over time by measuring the locations that channel traces intersect with a line perpendicular to channel paths (Supplementary Fig. 1). For most of the channels (Venable 2, Venable 3, Cosgrove, Thwaites, and Getz 2), a line was drawn approximately halfway down the channel length and approximately perpendicular to the overall channel direction. Three channels (Bach, Stange 2, and PIG) do not have persistent meanders along their length, but experience localized deflections in channel path related to fractures or other shifts that occur independent of ice flow. For these channels, the perpendicular line was drawn approximately halfway down the channel sections free from these deflections.

https://doi.org/10.1017/jog.2024.20 Published online by Cambridge University Press

Ice-flow-independent channel movement

The above analysis considers lateral channel movement as the result of all combined controls on channel paths, but it can be useful to decompose this movement into components that can be attributed to specific controls. We hypothesize that channel-path evolution is controlled jointly by ice-shelf flow and by other factors, such as ocean melt or gradients in surface accumulation. The contribution of ice flow to channel path migration can be determined by digitizing a channel location early in the record and then predicting the location and shape of the channel at a later time using an ice-flow velocity dataset. Any differences between the predicted location and the actual location as observed in Landsat imagery at the later time must be attributed to controls other than ice-shelf flow.

We carried out this analysis for each channel over a period of approximately 20 years (2000-2020), a time period coincident with velocity records available from MEaSUREs (Rignot and others, 2017) and ITS_LIVE (Gardner and others, 2019). While both of these datasets are accompanied by annual velocity products (Gardner and others 2019, Mouginot and others 2017), large spatial and temporal gaps precluded accurate point migration. We therefore were constrained to velocity grids averaged over the entire time period for point migration, and used the more limited annual products to measure trends in ice-flow speed and direction. As Thwaites Eastern Ice Shelf experienced exceptional changes in both speed and flow direction during this period, an annual velocity product produced for this ice shelf (Alley and others, 2021) was used for migrations at the Thwaites channel.

For each channel, points were placed at a 500 m spacing along the first channel digitization available after January 1, 2000. The points were allowed to migrate at a 1-day timestep through the velocity field until the time of the last available channel digitization, around the year 2020. Total estimated error in the migration ending locations was calculated as the sum:

$$\epsilon_{mig} = \epsilon_{base} + \epsilon_{rot} + \epsilon_{acc} + \epsilon_{dig} \qquad \text{(eq. 1)}$$

Here, $\epsilon_{base} = \Delta t * \epsilon_{vel}$, where ϵ_{vel} is the average estimated annual error in surface velocity along each channel provided by ITS_LIVE or MEaSUREs and Δt is the number of years over which the migration was carried out. Error associated with ice-flow rotation is calculated as $\epsilon_{rot} = \bar{u} tan\theta$, where $\bar{u}$ is the average ice-flow velocity along the channel and θ accounts for ice-flow rotation. To conservatively estimate a value for θ, we measured the change in ice-flow angle during the migration period at five points spaced evenly along each channel, and assigned the largest significant trend as the value for θ. Error associated with ice-flow acceleration is accounted for as $\epsilon_{acc} = 0.5 * \Delta t * a$, where a is the maximum annual acceleration observed along the channel. We multiply by 0.5 because much less than 50% of ice-shelf acceleration or deceleration is perpendicular to the direction of tracked basal channels (in other words, we are assuming that the angle between the ice-flow direction and the channel direction is less than 45˚), and our analysis relies on channel-path movement to left or right when the viewer is oriented along-flow. Error is therefore likely overestimated by this method, suggesting that our results showing evolution outside error bars are conservative estimates. Finally, we added the error associated with the channel path digitization, ϵ_{dig}, which is calculated as the

https://doi.org/10.1017/jog.2024.20 Published online by Cambridge University Press

root-mean square distance between investigator digitizations estimated for each channel as described above. Uncertainty estimates are provided as Supplementary Table 1.

As the Thwaites channel migration relied on a different velocity dataset, the error analysis was also slightly different. The Thwaites annual velocity dataset (Alley and others, 2021) accounts for changes in ice-flow speed and direction, so we did not need to account for that uncertainty in the error bars. However, estimates for the error associated with the velocity dataset were much higher, as the velocities were derived largely from lower-resolution MODIS data, particularly in the first 10 years of the record when relatively few MODIS images were available for correlation. Therefore, we limited the TEIS channel migration calculation to the period between 2010 and 2020, when error estimates are much smaller, giving the dataset greater utility. Because the TEIS is flowing very rapidly, signals in this reduced time period were large enough to fall outside the error bars. We note, however, that a 20-year channel trace migration revealed nearly identical results to the 10-year channel trace migration, suggesting that actual uncertainties in the velocity dataset and resulting channel positions are much lower than estimated.

RESULTS

Basal channel patterns

The basal channels surveyed are generally sub-parallel to ice flow, although most deviate from the ice-flow direction to at least some extent along their paths (Supplementary Fig. 1). The channel on the Bach Ice Shelf has a distinctive lateral deviation near the middle of the channel before returning to a path sub-parallel to flow in the lower reaches (Supplementary Fig. 1a). Three channels (Venable 1, Abbot, and Getz 1) have repeated lateral deviations along their entire lengths, and Stange 2 shows these characteristics in its upper reaches. These deviations resemble meanders observed in terrestrial surface streams, and generally persist throughout the Landsat record, although the meanders on Getz 1 become more strongly developed towards the second half of the Landsat record. While most of these meanders exhibit subtle changes throughout the record, some meander changes are large. For example, one meander on the upper section of Stange 2 that is present early in the record is bypassed starting around 2006, in a manner that appears to be analogous to a meandering stream cutting off an oxbow lake (Figure 2).

We can quantify these deviations in channel paths by calculating sinuosity. Sinuosity is defined as the channel center-line distance divided by the straight-line distance from the farthest upstream point (head) to the farthest downstream point (mouth) on the channel. Channels that are close to straight have sinuosity values very close to one, while channels with meanders or other deflections have sinuosity values larger than one. The channels fall into three sinuosity trend categories: increasing sinuosity (Pine Island, Getz 1, Getz 2), decreasing sinuosity (Stange 1, Thwaites, Venable 2, Venable 3), and sinuosity with no clear trend through time (Abbot, Bach, Cosgrove, Stange 2, Venable 1). Sinuosity plots for all channels are provided in Supplementary Fig. 2, while representative plots from each category are shown in Figure 3.

Many of the channels with high sinuosity or increasing sinuosity interact extensively with ice-shelf basal fractures and/or full-thickness rifts. For example, starting around 1997, a series of

https://doi.org/10.1017/jog.2024.20 Published online by Cambridge University Press

fractures developed downstream of the large ice rise that deflects ice flow at Stange 2 (Figure 2). These fractures captured and deflected the basal channel, and the channel was observed to move to newer upstream fractures as ice advection shifted older fractures downstream. Getz 1 showed a similar progression towards more meanders over time through deflection into fractures.

In contrast, the basal channel observed on Thwaites Eastern Ice Shelf ceased visible interactions with ice-shelf fractures as it developed (Figure 4). Images from early in the record show a sinuous channel with abrupt directional changes that appear to follow ice-shelf fractures. Over time, the fractures were advected and calved off the ice-shelf front, leaving a smoothly curving channel that closely follows the ice-flow direction. This smooth pattern developed gradually as what appears to be a relatively stationary basal-channel-initiation site generated ocean plumes that carved a preferential path through the ice shelf moving above. Despite ice-shelf fractures penetrating across the Thwaites channel from 1973-2013 and fractures reaching the channel on one side after 2013, the Thwaites basal channel does not appear to have been deflected into any of these fractures.

Only a few channels experienced clear upstream or downstream channel-head migration during the study period. The heads of ocean-sourced basal channels can be difficult to pinpoint because they tend to be diffuse and may be obscured by fractures. However, two channels showed clear headward growth during the study period: Pine Island Glacier (PIG; Figure 5a) and Getz 2 (Supplementary Fig. 1c). The path of the PIG channel clearly followed a fracture along some of its new, upstream channel length. Both PIG and Getz 2 experience an increase in sinuosity over time as their upper reaches extend in new directions, which could be the result of new channel growth, of background ice-shelf thinning allowing channel segments to become visible through the reduction of bridging stresses (Drews 2015), or both. All channels selected for this study terminate at the ocean, so their downstream extent is controlled by changes at the ice-shelf calving front.

Lateral channel-path movement over time

Lateral channel-path movement over time was quantified by observing intersections with a fixed perpendicular line, as described in Methods. Intersections with this perpendicular line were calculated for each set of channel traces, and their distances from the first channel trace were plotted through time. The results are shown in Figure 6 for investigator one, and Supplementary Fig. 3 for investigator two. Error bars for each channel location include digitization errors and the uncertainty associated with ice-flow rotation, as discussed in Methods. As the perpendicular transects were selected at locations where the channel parallels ice flow, ice-flow acceleration/deceleration should not contribute to these error bars, which relate to lateral channel movement. The results show that most of the channel traces moved to the left (when looking downstream) outside error bars over time. For some channels, such as Bach, this movement is relatively steady throughout the record, which began in the early 1970s for this channel. Others, such as Thwaites, appear to experience changes in the rate of movement over time. Only the PIG channel appears to move significantly to the right over time, while Cosgrove is the only channel that does not show clear migration outside error bars in either direction.

https://doi.org/10.1017/jog.2024.20 Published online by Cambridge University Press

Lateral channel-path movement independent of ice flow

The results in the previous section reflect lateral channel movement due to the combined influence of ice flow, basal melt, and surface processes. By using independent records of ice-flow velocity, we can account for lateral channel movement due to ice flow, and the remainder represents the component of lateral channel movement due to the effects of basal melt or surface processes. After predicting channel locations using ice-flow velocity datasets (see Methods and Supplementary Fig. 4), we calculated the percentage of channel length observed to lie to the left or right of the predicted locations when facing down-channel. Migration to the left or right is considered to be significant if it falls outside estimated error bounds.

Migrations for all channels are shown in Supplementary Figures 4 (MEaSUREs) and 5 (ITS_LIVE). As an example, the second panel in Figure 5b shows the original, predicted, and observed paths for a channel migration on PIG between January 2001 and September 2019, along with the full set of channel traces over this time period in Figure 5a. Despite the rightward lateral migration observed in the raw channel traces in Figure 5a, accounting for ice flow shows that the flow-independent channel migration is primarily to the left. Percentages of channel length observed to migrate significantly to the left and right are shown for each channel in Figure 7 (lateral migration including both significant and insignificant changes are shown in Supplementary Fig. 6), and the results show that the basal channels in this study have migrated overwhelmingly to the left of ice flow.

DISCUSSION

Growth, evolution, and sinuosity changes

The results presented here give insights into nearly five decades of evolution of ocean-sourced channels in a region experiencing changing ocean and ice-dynamical forcings. The most pronounced changes were observed on PIG and Thwaites, the two locations within our study region where mCDW forcing is expected to be largest (Scambos and others, 2017; Nakayama and others, 2019). In both cases, our analysis suggests that the channels first formed just before our record began, and we observe significant changes in length and sinuosity over time. Although we started our digitizations on PIG in 1989, when the tracked channel first reached the ice edge, Landsat imagery captured the early growth of this channel starting in 1973 (Figure 5). Initially, the channel was approximately straight. The surface expression of the channel grew downstream, developing a smoother path over time and reaching the ice edge by 1989. Following this formation, the channel then began a rapid headward growth around 2001, adding another upstream segment at a new angle starting around 2017. The 2017 growth follows a fracture that is part of a series of fractures forming downstream of the grounding zone. In many cases there is a continuum between channels and fractures (e.g. discussed by Bindschadler and others, 2011, Dutrieux and others 2013), making it difficult to distinguish the two based on surface expression alone. Time series are often useful in distinguishing relationships, as in this case where we see the channel grow upstream and meet seamlessly with one of a set of fractures. This headward extension is similar in style to the much smaller headward growth observed on Getz 2 starting in the 1990s, as well as the headward growth on another channel on the Getz Ice Shelf observed by Alley and others (2016). In all three cases, the headward

https://doi.org/10.1017/jog.2024.20 Published online by Cambridge University Press

growth did not occur in a smooth line, but experienced abrupt deflections from the ice-flow direction, which may be consistent with influence by basal fractures or other irregularities in basal topography. Just as surface streams opportunistically flow into low spots, buoyant plumes beneath ice shelves opportunistically flow into high spots, such as thin shear margins (Alley and others, 2019) or other basal topography (Gladish and others, 2012). Although drawn from a very limited number of observations, this suggests that young channels may be likely to have relatively high sinuosity as they deflect through basal fractures.

We note that the growth of the surface expression of a channel may or may not be precisely concurrent with the growth of the channel on the base of the ice shelf. The surface expression of a basal channel is the result of hydrostatic relaxation of the ice over the channel. When channels are narrow compared to the ice thickness, bridging stresses may reduce or prevent this hydrostatic relaxation (Drews 2015, Stubblefield and others 2023). This implies that background thinning of an ice shelf could increase the surface expression of a basal channel, even if the channel itself is not growing, an effect that could be responsible for the appearance of channel lengthening. The rapid headward growth of the large channel on Getz Ice Shelf reported by Alley and others (2016) and explored in more detail by Chartrand and Howat (2020) was accompanied by both background ice-shelf thinning and rapid channel deepening. More detailed work is needed to assess the relative contributions of background ice-shelf thinning and channel growth to the appearance of channel change.

The new channel growth observed on PIG and Getz gives us context to interpret the formation of the channel on Thwaites. In the first Landsat image available, from 1973 (Figure 3), the Thwaites channel had a relatively faint surface expression, suggesting that the channel had not yet carved deeply into the base of the shelf along its entire length. The channel also followed a highly sinuous path connecting large fractures that are visible on the surface. This is consistent with a young channel, and is observed at the same time as the channel on PIG was first forming (Figure 4). To test the hypothesis that the Thwaites channel had formed relatively recently in 1973, we used oblique air photos available from United States Geological Survey Earth Resources Observation Science Center Archive that were collected in 1947 and 1966 (map shown in Supplementary Fig. 9; images shown in Supplementary Videos 1-6). One flight line imaged the Thwaites Eastern Ice Shelf in 1947, and three - from three different angles - are available from 1966. Although the surface expression of fractures and other surface undulations are clearly visible on the ice-shelf surface in the imagery, even in the 1966 imagery we see no evidence of the large, sinuous depressions, comparable in scale to observed fractures, that are expected to be present in the central ice shelf if the channel had developed by this time. Although not conclusive, this evidence suggests that the Thwaites channel likely first formed between 1966 and 1973.

As the young Thwaites channel developed, the plume, which maintained a relatively stationary origin point at the head of the channel, gradually carved a preferential path through the advecting ice above, developing towards a mature channel path much closer to the ice-flow direction. Simultaneously, large deviations in channel direction due to opportunistic plume flow through fractures were advected off the ice shelf, while extensional ice-shelf flow additionally

https://doi.org/10.1017/jog.2024.20 Published online by Cambridge University Press

stretched remaining channel-direction deviations. The result was a large decrease in sinuosity over time (Figure 3).

Several other channels (Venable 1, Venable 2, Venable 3, and Stange 1) also showed a decrease in sinuosity throughout the record (although of a much smaller magnitude than the extreme example at Thwaites; see Supplementary Fig. 2) suggesting that they may also have been relatively young channels when our record began in the 1970s and are moving towards some sort of steady-state. However, other channels (Getz 1, Getz 2, and PIG) showed small increases in sinuosity during this time period. As noted, Getz 2 and PIG experienced visible headward growth, demonstrating that they are actively evolving systems. Getz 1 has shown increased interaction with fractures over time, as sections of the channel have been deflected into and out of these fractures. The upper reaches of this outflow of the Getz Ice Shelf experienced some of the highest thinning rates in Antarctica between 1994 and 2012 (Paolo and others, 2015), and our time series show new fractures forming around the tracked channel throughout this time period (Supplementary Fig. 7). Rapid background ice-shelf thinning at Getz and elsewhere may also reduce bridging stresses and allow new sections of a channel to become visible.

These examples suggest that channel life cycles can be reset or rejuvenated through evolving ocean forcing or structural changes in the ice shelf, which are often the result of dynamic thinning and basal melt. Stange 2 (Figure 2) also interacts extensively with fractures during the second half of the record, but its sinuosity trends are less clear because of the upstream meander cutoff early in the record, while sinuosity increased in the lower half of the channel due to capture by fractures. The sinuosity of the channels on Bach, Abbot, and Cosgrove showed no clear trends through the record. We note that all three of these ice shelves are relatively slow-flowing, leaving little opportunity for directional deviations in channel paths to calve off the ice shelf and lowering the effects of ice-shelf spreading on meander shape.

Evidence of ocean control

Basal-channel evolution is controlled by complex interactions between ice flow, ocean forcing, ice-shelf structural features, and surface accumulation patterns. Alley and others (2016) showed that basal-channel density is correlated with ice-shelf basal melt rate, and that ice shelves in the ABS with deeper grounding lines had higher basal-channel densities, suggesting that increased interaction with mCDW leads to more basal channels. These results indicate a strong oceanic control on the development of basal channels.

The data presented in this study show that ice-flow-independent lateral channel path migration is dominantly controlled by ocean processes, aside from perturbations due to interactions with ice-shelf structural features (which themselves are usually forced by ocean change in the ABS). Figure 7 shows the lateral migration direction of the basal channels in this study independent of ice flow during our study period. Lateral channel migration outside of error bars is overwhelmingly to the left when facing downstream. This is consistent with Coriolis deflection to the left in the Southern Hemisphere, and strongly suggests that basal melt is primarily responsible for this flow-independent lateral migration. Sergienko (2013) showed in an ocean

https://doi.org/10.1017/jog.2024.20 Published online by Cambridge University Press

model that plume flow and basal melt are significantly higher on the Coriolis-favored (left-hand) side within basal channels, and predicted that basal channel paths should deflect to the left of ice flow when forced by ocean plumes influenced by Coriolis deflection. Alley and others (2016) also observed that many channels have asymmetric profiles with steeper slopes on the left-hand side, consistent with Sergienko (2013) and higher basal melt rates on that side. While surface-accumulation patterns also likely play a role in lateral channel migration (Drews and others, 2020), the consistency of this directional shift among channels of varying orientations over a wide geographic area in this study suggests that the ocean is the dominant control on lateral migration of large, unconfined channels in the ABS sector.

Verification of leftward channel migration using radar profiles

The remote-sensing-based analysis of flow-independent lateral migration presented above, which essentially allows for the comparison of channel paths in a Lagrangian framework, can be independently verified using ice-penetrating radar. The stacked layers observed in a radar profile have moved as a Lagrangian parcel with ice flow, while new layers have been added to that parcel over time with snow accumulation. Those accumulating layers will, barring significant wind redistribution, accumulate sub-parallel to the ice-shelf surface, preserving the contours of the surface expression of a basal channel as it moves laterally across the ice shelf over time due to asymmetric basal melt rates. To test this hypothesis, we obtained airborne ice-penetrating-radar profiles of the IceBridge snow and accumulation radars for Venables 1-3, Abbot, and Thwaites (Supplementary Fig. 8), which were the available profiles that crossed a basal channel in this study and clearly showed the layers of the upper ice shelf. An example profile from Venable 1 is shown in Figure 8. The profiles confirm the leftward movement of the channels through time, as well as the expected asymmetric profile showing a steeper slope on the Coriolis-favored side of each channel. This supports the dominance of basal melt in controlling ice-flow independent lateral channel migration, which was inferred based on the leftward lateral migration direction overwhelmingly observed in this study.

We note that the basal channels in the study typically do not appear to widen perceptibly as they migrate through the ice shelf, which may indicate that convergent ice flow into basal channels, which has been observed in satellite data (Drews, 2015) and ice-flow models (Wearing and others, 2021), may approximately balance total lateral basal melt. In fact, the balance between the rate of lateral Coriolis-influenced basal melt through the ice shelf and the rate of ice-flow creep filling the channel likely together set the channel width. The radar profiles crossing basal channels show that channel widths do not appear to systematically change through time. However, due to the diffuse nature of channel boundaries in optical satellite imagery, we were unable to measure basal-channel widths through the full record with sufficient confidence for this study. Further work on basal-channel widths and their changes through time remains to be completed in the future.

Conceptual model of steady-state channel paths

We can interpret systematic changes in the shape and location of channel paths by using a conceptual model of channel-path evolution. Based on our discussion above, our data show that the evolution of channels in this study is dominated by ice-shelf flow and basal melt, and that

https://doi.org/10.1017/jog.2024.20 Published online by Cambridge University Press

basal melt is influenced by increased melt rates on the Coriolis-favored (left-hand) side. For this conceptual model, we will assume that these are the only two significant controls on channel paths, which is at least approximately consistent with our data.

First, consider the path of the apex of a basal channel that forms on an idealized ice shelf with steady-state, uniform flow in a world without Coriolis (Figure 9a). Due to ice-shelf spreading, ice-shelf flow tends to be slower at the grounding line and faster approaching the calving front, as represented by the black vertical arrows in Figure 9. In the figure, a parcel of ice moves over the top of a newly formed ocean plume that begins carving a basal channel. We will also assume that this plume is in steady-state; i.e. the volume of water involved, the speed of the plume, and the thermal forcing available remain the same over time.

In this steady, no-Coriolis world, the ocean plume will carve an indentation in the parcel of ice currently at the head of the channel, and the channel apex will be advected straight towards the ice edge. As the channel apex advects, the plume must begin to carve into a new parcel of ice at the head of the channel in an Eulerian manner, extending the indentation. In this way, the channel lengthens in a straight line towards the ice edge (light blue bold line in Figure 9a, dashed light blue bold line for reference in panels b-f). As the ocean plume preferentially flows through the lengthening indentation, melt may continue to deepen the indentation in previous parcels of ice, opposed to varying degree by the tendency of ice creep to close the channel (Wearing and others, 2021). Observations of many basal channels that are maintained or even deepen towards the ice-shelf edge (Alley and others, 2016) show that plumes commonly maintain sufficient melting and/or creep is sufficiently slow to allow the channels to remain open. Any given parcel of ice that becomes part of the channel on this steady-state ice shelf with the steady-state plume will experience the same amount of melt and creep during its journey from the grounding line to the calving front; as one parcel of ice is advected away by ice flow, a new parcel of ice replaces it, and the new parcel is subject to the same amounts of melt and creep. This balance between steady ice-shelf flow and steady plume-induced melt creates a steady-state channel path parallel to ice-shelf flow and with a depth profile at the apex that is consistent in time.

Now consider a more realistic world, where the ocean plume is influenced by Coriolis deflection (Figure 9b). Models show (e.g. Sergienko 2013) that we should expect higher plume-flow velocities on the Coriolis-favored side of the channel (the left-hand side in the Southern Hemisphere). Since melt rate increases with the water flow speed (e.g. Jenkins and others 2010), this Coriolis deflection causes increased melt on the left-hand side of the channel. We will assume that the ice shelf maintains steady-state ice flow, as in the previous conceptual model. We will also continue to assume that the plume remains steady. With a steady-state plume on an idealized ice shelf, the amount of Coriolis-influenced melt should decrease towards the ice edge, because the plume is expected to be fastest and close to the ice near the channel head where the ice-base slope is steepest, and to lose energy and perhaps detach from the ice-shelf base when traveling along the flattening base of the ice shelf towards the calving front (e.g. Dutrieux and others, 2013), and because both Coriolis influence and melt rates are

https://doi.org/10.1017/jog.2024.20 Published online by Cambridge University Press

expected to decrease when flow rates decrease. This Coriolis-influenced melt is represented by the horizontal magenta arrows in Figure 9.

Once again, consider the path of a channel apex under this balance of steady-state forcings (Figure 9b). As a parcel of ice passes over the plume origin, it will once again carve an indentation into the ice-shelf base, and that indentation will once again be advected downstream. However, this time as the plume continues to melt and maintain the open channel, it preferentially melts on the Coriolis-favored side and leaves the other side to be filled in by ice creep. As the channel advects downstream, the position of the apex is now shifted slightly to the left of the location predicted by ice flow. From this new position, the indented parcel of ice will continue to advect downstream, continue to be influenced by Coriolis-influenced melt, and continue to be shifted to the left of ice flow. However, this continued shift is limited to individual parcels of ice. The channel as a whole will not indefinitely migrate to the left on a steady-state ice shelf with a steady-state ocean plume because every parcel of ice is subject to a finite and equal amount of Coriolis-influenced melt during the time it advects across the ice shelf; a parcel that melts farther sideways through the shelf due to Coriolis must also advect farther down the shelf due to ice flow. In other words, a balance will be developed between the steady Coriolis-induced melt and steady ice-shelf flow that determines the ultimate shape of a steady-state channel path (dark blue bold line in Figure 9b, dashed dark blue bold line for reference in panels c-f).

It is worth noting that the lateral difference in channel path from the ice-flow direction is expected to be relatively small, and the scale is highly exaggerated in Figure 9. Supplementary Text 1 presents a mathematical analysis of steady-state channel shapes on ice shelves with constant and varying ice flow and a steady melt rate. This analysis shows that the scale governing the lateral deviation of a channel path from the ice-flow direction is set by the melt rate over the ice-flow velocity, which would typically be a very small number.

Little work has been done on the balance of forcings that allows a plume to essentially melt sideways through an ice shelf in the Coriolis-favored direction while the channel is filled in at a comparable rate by ice creep on the other side and advected with the ice flow, which would result in a steady-state channel path under ideal conditions. However, there is ample observational evidence to show that this is realistic, even if the exact mechanisms have not been fully quantified. Satellite-derived digital elevation models show lateral channel migration on the Getz Ice Shelf in a Lagrangian sense, with ice on the left side of a channel melting preferentially over time (Chartrand and Howat, 2020), and radar data of subsurface layers similarly show progressive channel migration on the Roi Baudouin Ice Shelf (Drews and others, 2020). Our analysis above removes the ice-flow signal to reveal flow-independent lateral channel migration, which is also visible in the radar layers presented here (Figure 8, Supplementary Fig. 8). In all observed cases, a visual analysis over years to decades of data shows that the channels maintain an approximately steady width over time, suggesting that lateral melt and creep approximately balance each other under most conditions, and the width of the channel is likely set by this balance between lateral melt and ice creep, interacting with spatially variable snow accumulation.

https://doi.org/10.1017/jog.2024.20 Published online by Cambridge University Press

Conceptual model of channel change under non-steady forcings

Now that we have established a model of a steady-state channel profile as controlled by ice flow and Coriolis-influenced ocean melt, we can consider the expected evolution of channel paths - such as the Landsat-based time-series we have developed in this study - under non-steady forcings. First consider a basal channel under the influence of a steady-state ocean plume with steady-state Coriolis-influenced melt on a decelerating ice shelf (Figure 9c). In this scenario, the rate of Coriolis-influenced melt (the magenta arrows) across the shelf remains the same as in the previous panels, but the black arrows representing ice-flow speed get smaller. The resulting new channel path, shown in green, is shifted to the left of the steady-state profile. If ice-flow deceleration continues, a time series of channel paths would continue to be shifted to the left of the previous channel paths. Figure 9d shows that ice-flow acceleration yields the opposite result: an increase in the length of the black vectors representing ice-flow speed causes the new channel path, again in green, to shift to the right of the steady-state channel path, and if acceleration continues, a time-series of channel paths will continue to be shifted to the right of the previous path.

In Figures 9e-f ice-flow speed is held constant in time, as in the steady-state profiles in a and b, but the Coriolis-influenced melt is varied. In turbulent settings, melt rates change based on the speed of water flow and the heat content of the plume (e.g. Jenkins, Nicholls, and Corr, 2010). Lateral melt on the Coriolis-favored side would increase if the plume gains velocity and/or heat content, which could both be due to more vigorous circulation caused by an increase in warm-water availability or runoff. Coriolis-influenced melt would decrease if the plume loses velocity or heat content, which could be due to decreased warm-water availability. In Figure 9e, an increase in Coriolis-influenced melt is indicated by a lengthening of the horizontal magenta vectors, which results in a shift of new channel paths to the left of old channel paths. A decrease in Coriolis-influenced melt, shown in Figure 9f, results in channel paths being shifted to the right.

Based on this conceptual model, time-series observations of channel paths that move to the right of the previous path could indicate ice-flow acceleration and/or a decrease in Coriolis-influenced melt. If channel paths are shifted to the left over time, this would indicate that ice flow is decelerating and/or Coriolis-influenced melt is increasing. We note that both of these trends could be confounded by ice-flow rotation, but we account for ice-flow rotation in our error bars, as described in our Methods section. All of the trends discussed in the next section fall outside of error bars.

Non-steady behavior in our observed channel paths

Based on the conceptual models above, ice flow and ocean-induced melt together explain the time-evolution of the basal-channel paths in this study. Of those three variables, we can directly observe ice flow and channel paths, and by constraining those, infer changes in ocean-induced melt. We note that the conceptual model described above is much more difficult to apply in cases of meandering channel paths. Advection of meanders (which may represent steady-state conditions or exhibit a trend over an observational period of many decades to centuries) can obscure channel-path trends on timescales of a few decades. We therefore exclude the

https://doi.org/10.1017/jog.2024.20 Published online by Cambridge University Press

Venable 1, Abbot, and Getz 1 channels from the following discussion. We also exclude Stange 1 (Supplementary Fig. 1a), because it does not follow the parameters of the conceptual model, which requires that ocean flow and ice flow are in approximately the same direction.

As noted in the Methods section, we used the MEaSUREs (Mouginot and others, 2017) and ITS_LIVE (Gardner and others, 2019) annual velocity data to extract significant trends in ice-flow speed, and reported the largest trend along each channel for inclusion in error estimates (Supplementary Table 1). This analysis showed that Bach, Cosgrove, and Venable 2 did not experience a significant change in flow speed during the study period. The remaining channels being considered in this discussion - Getz 2, PIG, Stange 2, Venable 3, and Thwaites - all experienced significant accelerations in ice-flow speed. Based on these observations, if ocean melt remained in steady-state during the study period, we would expect the channel paths for Bach, Cosgrove, and Venable 2 to fall directly on top of each other (representing steady-state ocean melt and steady-state ice flow), while Getz 2, PIG, Stange 2, Venable 3, and Thwaites would show movement to the right over time (representing steady-state ocean melt and accelerating ice flow).

Only two of the channels largely followed these predictions. The channel paths for Cosgrove consistently overlap and show no clear trend of movement over time. We therefore consider Cosgrove to be an example of a channel that has been approximately in steady-state with respect to both ice flow and ocean melt throughout the study period. The channel paths for PIG moved primarily to the right over time, particularly near the head of the channel, which is consistent with accelerating ice flow. The lowest reaches of Stange 2 also showed movement to the right consistent with accelerating ice flow.

However, Bach, Getz 2, the upper reaches of Stange 2, Thwaites, Venable 2, and Venable 3, had channel paths that migrated to the left over time. On Bach and Venable 2, where velocities are approximately stable, this must represent increasing ocean-induced melt over time, if we accept the evidence presented here that increased plume forcing is likely to be the main control on flow-independent lateral channel movement. On Getz 2, Stange 2, Thwaites, and Venable 3, accelerating ice flow should be pushing channel profiles to the right, but instead they are moving to the left over time. Therefore, the increased plume-melt signal has dominated the ice flow signal, indicating a strongly non-steady ocean forcing over time.

We note that changes in subglacial hydrologic discharge might also have an impact on the paths of basal channels that are driven by channelized subglacial plumes. We have limited our analysis to ocean-sourced channels, which originate downstream of the grounding line, decreasing the likelihood that they are directly influenced by subglacial discharge. However, changes in subglacial discharge can also change the overall thermal forcing in an ice-shelf cavity (e.g. Wei and others, 2020), and an increase in subglacial discharge could cause the same leftward channel migration that we have observed in this study. As discussed in the following section, our observations are consistent with a collection of independent data sources suggesting increased ocean forcing from mCDW intrusion, and this is the most likely forcing to influence the ocean-sourced channels in this study.

https://doi.org/10.1017/jog.2024.20 Published online by Cambridge University Press

Basal channels as evidence for non-steady ocean forcing in the ABS

All of these lines of evidence indicate a changing ocean forcing throughout much of the ABS during our study period. Since none of the ice-shelf areas with channels in this study have experienced a recent decrease in velocity, leftward migration of channel paths indicates increased melt on the Coriolis-favored side of the channels, suggesting more rapid plume flow, warmer waters within plumes, or both. As shown in Figure 6, non-steady leftward channel migration was observed on Bach, Venable 2, and Getz 2 from the start of the record in the 1970s, and on Thwaites, Venable 3, and Stange 2 by the 1980s or early 1990s. As described above, this signal can be confounded by the impacts of acceleration in ice flow deflecting channels to the right. Reliable velocity records prior to the 1990s are generally unavailable, but if obtainable, they could be used to better constrain signals of non-steady ocean forcing found in channel-path change. Other observations of basal channel change may also indicate changing ocean forcing. PIG and Thwaites, for example, both experienced growth of new channels in the 1970s, which likely also indicates a change in ocean forcing. This means that, from the start of our record in the early 1970s, we have evidence of an increase in ocean-induced melt in basal channels across our entire study region, as bounded by Bach in the east and Getz 2 in the west. This forcing is likely to have been spatially heterogeneous, but was widespread enough to also affect Venable 2, Thwaites, and PIG from early in the record. Our results do not rule out non-steady ocean forcing at other locations due to the possibility of ice-flow changes or surface processes confounding the signal.

Lateral basal channel migration is a novel proxy that contributes to a large and growing body of literature tracing the change in ocean forcing that initiated thinning and retreat of ABS ice shelves during the 20th century. Much evidence is available since the 1990s, when altimetry became widely available, that corroborates the reliability of this proxy. Paolo and others (2015) mapped thinning rates on ice shelves around Antarctica between 1994 and 2012, which spans a large subset of our study period. During this time, every ice shelf included in our study thinned significantly with the exception of Cosgrove, which experienced 0% thinning between 1994 and 2012 (Paolo and others, 2015). Cosgrove is the only channel observed in our study with steady-state behavior. Abbot's thinning was only 1% when spatially averaged during the same time period, but this average is weighted by a large expanse of the ice shelf experiencing very slow thinning rates. The outflow containing the basal channel included in this study thinned substantially faster between 1994 and 2012 (Paolo and others, 2015), at rates similar to the Venable Ice Shelf just to the east. This correspondence is supported by Adusumilli and others (2020), who calculated basal-melt rates on ice shelves between 1994 and 2018. Of the ice shelves with basal channels included in our study, the only ice shelf measured as producing no excess meltwater was Cosgrove (0 +/-4.1 Gt/yr; Adusumilli and others, 2020). Our results support these altimetry-based studies by showing that ice shelves with high thinning rates and excess melt are associated with channels that are exhibiting non-steady behavior.

Evidence of change in ocean forcing in remote sensing data before the altimetry record is harder to find. Christie and others (2016) found evidence in Landsat imagery of grounding-line retreat on Stange in the 1970s, and several other ice shelves in the Bellingshausen Sea in the

https://doi.org/10.1017/jog.2024.20 Published online by Cambridge University Press

1980s. In addition, our observations support previous work demonstrating decades of change on PIG and Thwaites. Landsat imagery indicated that PIG lost contact with a seabed ridge in the mid-1970s (Jenkins and others, 2010), a change that occurred just after the formation of the basal channel on PIG (Figure 4) and the inferred formation time of the channel on Thwaites. Our results are consistent with these Landsat-based studies, but our basal channel proxy evidence for ocean-forcing change during or before the early 1970s expands these implications over a greater spatial extent.

Ocean forcing in the decades before the Landsat record is even harder to constrain, but insights can be gained from models and ocean sediment cores. Steig and others (2012) suggested, based on ocean modeling results, that the Amundsen Sea ocean forcing may have responded to changes in tropical sea-surface temperatures in the 1940s, initiating changes in ice-sheet dynamics that continue today. Several sediment cores from Pine Island Bay suggest that ocean forcing may have increased in that region as early as the 1940s (Hillenbrand and others, 2017; Smith and others, 2017), with unpinning of the Pine Island Ice Shelf from a seafloor ridge around 1970 (Smith and others, 2017) leading to greater mCDW circulation beneath the shelf. This is coincident in time with the formation of the new PIG basal channel shown in Figure 4. New data from ocean sediment cores in front of Thwaites (Clark and others, in press) also point to the 1940s or earlier for the initiation of ice-shelf thinning, and show that grounding-zone retreat began in the 1950s. Our results suggest that the large basal channel on Thwaites first formed in the late 1960s, after this grounding-zone retreat was underway. A sediment core in front of the eastern Getz Ice Shelf (Kim and others, 2021) recorded an abrupt increase in bio-productivity around 1970.The authors attributed the change to greater nutrient input from increased ice-shelf basal melt associated with the onset of enhanced mCDW inflow at that time. While these cores are spatially limited, our results support their findings and suggest that the enhanced ocean forcing was widespread in the ABS by at least the 1970s and 1980s, with direct impacts on ice-shelf basal melt through basal channel formation and evolution. While our observations begin with the Landsat record, our conclusions do not preclude basal channel change in previous decades, and thorough analysis of historic air photos may yield further insights starting in the 1940s.

Conclusions

Our results indicate that basal-channel evolution serves as a novel proxy for changing ocean forcing throughout the optical satellite imagery record. Our results are consistent with previous work presenting evidence of oceanic changes in portions of the ABS in the 1970s or earlier. In particular, our results clearly demonstrate ocean changes and new ice-ocean interaction patterns at Thwaites and Pine Island Glaciers by the late 1960s or early 1970s. Pervasive basal-channel change throughout the ABS channels in this study indicates that this enhanced ocean forcing was widespread starting at least in the 1970s.

Our results also help illuminate aspects of the formation and life cycle of basal channels. Newly-formed ocean plumes tend to opportunistically flow through high spots in the ice-shelf roof of the ocean cavity, and therefore often take advantage of basal fractures. The resulting channel paths are highly sinuous. Ice-shelf stretching accompanied by advection and calving of these

https://doi.org/10.1017/jog.2024.20 Published online by Cambridge University Press

deflections in channel direction lowers basal channel sinuosity over time in the absence of other influences. These influences may include changes in ice-shelf flow due to thinning or interactions with pinning points, or the formation of new fractures that capture basal-channel-plume flow. These processes may reset channels and increase sinuosity. Not all basal-channel plumes appear to interact with basal fractures, however, and much more work remains to be done on basal-channel-plume dynamics.

Basal channels advect with ice-shelf flow, but their paths also migrate in response to surface and basal forcings. The channels in this study experienced overwhelmingly leftward channel migration independent of ice flow, which is the Coriolis-favored direction. These results strongly indicate that the ocean is the primary driver of lateral basal-channel migration independent of ice flow in the ABS, and lend support to previous work that suggests that basal-channel formation and evolution is strongly controlled by ocean processes.

Basal channels serve both as sentinels of ice-shelf change and key players in ice-shelf stability. These features respond to and affect patterns of basal melt and ice-shelf strength, making them important components in future ice-shelf models. The widespread non-steady behavior of basal channels observed in this study indicates the need for continued monitoring and research into the processes that control these features.

Acknowledgements:
We thank members of the TARSAN Project, a component of the International Thwaites Glacier Collaboration (ITGC), for input on the ideas in this manuscript. This paper is ITGC contribution No. ITGC-076. We also thank Drs. Eric Steig, Julia Wellner, and Rob Larter for their comments. Authors of this work were supported by grants from the Natural Sciences and Engineering Research Council (CAN) grants RGPIN-2021-02910, RGPIN-2020-05689, and Canada-150 and CERC Research Chair Programs, NASA (USA) grants 80NSSC22K038 and 80NSSC22K0384, National Science Foundation (USA) grants PLR-1738934 and PLR-1929991, and National Environmental Research Council (UK) grants NE/S006672/1and NE/S006419/1.

Works cited:

Adusumilli S, Fricker HA, Medley B, Padman L and Siegfried MR (2020) Interannual variations in meltwater input to the Southern Ocean from Antarctic ice shelves. *Nature Geoscience,* **13**(9), 616–620 (doi:10.1038/s41561-020-0616-z)

Alley KE, Scambos TA and Alley RB (2023) The role of channelized basal melt in ice-shelf stability: recent progress and future priorities. *Annals of Glaciology*, 1–5 (doi:10.1017/aog.2023.5)

Alley, KE and 15 others (2021) Two decades of dynamic change and progressive destabilization on the Thwaites Eastern Ice Shelf. *The Cryosphere*, **16**(2), 397-417 (doi:10.5194/tc-15-

5187-2021)

Alley KE, Scambos TA, Alley RB and Holschuh N (2019) Troughs developed in ice-stream shear margins precondition ice shelves for ocean-driven breakup. *Science Advances*, **5**, eaax2215 (doi:10.1126/sciadv.aax2215)

Alley KE, Scambos TA, Siegfried MR and Fricker HA (2016) Impacts of warm water on Antarctic ice shelf stability through basal channel formation. *Nature Geoscience* **9**(4), 290–293 (doi:10.1038/ngeo2675)

Alley RB and 7 others (2014) Oceanic Forcing of Ice-Sheet Retreat: West Antarctica and More. *Annual Review of Earth and Planetary Sciences,* **43**(1), 1–25 (doi:10.1146/annurev-earth-060614-105344)

Bell RE and 9 others (2017) Antarctic ice shelf potentially stabilized by export of meltwater in surface river. *Nature,* **544**(7650), 344–348 (doi:10.1038/nature22048)

Bindschadler R, Vaughan DG, and Vornberger P (2011) Variability of basal melt beneath the Pine Island ice shelf, West Antarctica. *Journal of Glaciology*, **57**(204), 581-595 (doi: 10.3189/002214311797409802)

Chartrand AM and Howat IM (2020) Basal Channel Evolution on the Getz Ice Shelf, West Antarctica. *Journal of Geophysical Research: Earth Surface,* **125**(9), e2019JF005293 (doi:10.1029/2019jf005293)

Christie FDW, Bingham RG, Gourmelen N, Tett SFB and Muto A (2016) Four-decade record of pervasive grounding line retreat along the Bellingshausen margin of West Antarctica. *Geophysical Research Letters,* **43**(11), 5741–5749 (doi:10.1002/2016gl068972)

Clark and 17 others (in press, 2023) Synchronous retreat of Thwaites and Pine Island glaciers in response to external forcings in the pre-satellite era. *Proceedings of the National Academy of Sciences*, accepted

De Rydt J, Reese R, Paolo FS, and Gudmundsson GH (2021) Drivers of Pine Island Glacier speed-up between 1996 and 2016. *The Cryosphere*, 15, 113-132 (doi: 10.5194/tc-15-113-2021)

Dow CF and 8 others (2018) Basal channels drive active surface hydrology and transverse ice shelf fracture. *Science Advances,* **4**(6), eaao7212 (doi:10.1126/sciadv.aao7212)

Drews R, Schannwell C, Ehlers TA, Gladstone R, Pattyn F and Matsuoka K (2020) Atmospheric and Oceanographic Signatures in the Ice Shelf Channel Morphology of Roi Baudouin Ice Shelf, East Antarctica, Inferred From Radar Data. *Journal of Geophysical Research: Earth Surface,* **125**(7), e2020JF005587 (doi:10.1029/2020jf005587)

Drews R and 9 others (2017) Actively evolving subglacial conduits and eskers initiate ice shelf channels at an Antarctic grounding line. *Nature Communications,* **8**(1), 15228 (doi:10.1038/ncomms15228)

Drews R (2015) Evolution of ice-shelf channels in Antarctic ice shelves. *The Cryosphere,* **9**(3), 1169–1181 (doi:10.5194/tc-9-1169-2015)

Dupont TK and Alley RB (2005) Assessment of the importance of ice-shelf buttressing to ice-sheet flow. *Geophysical Research Letters,* **32**(4), L04503 (doi:10.1029/2004gl022024)

Dutrieux P and 6 others (2013) Pine Island Glacier ice shelf melt distributed at kilometre scales. *The Cryosphere,* **7**(5), 1543–1555 (doi:10.5194/tc-7-1543-2013)

Fürst JJ and 6 others (2016) The safety band of Antarctic ice shelves. *Nature Climate Change,* **6**, 479–482 (doi:10.1038/nclimate2912)

Gardner AS, Fahnestock MA and Scambos TA (2019) ITS_LIVE Regional Glacier and Ice Sheet Surface Velocities. *Data archived at the National Snow and Ice Data Center* (doi:10.5067/6ii6vw8llwj7)

Gladish CV, Holland DM, Holland PR and Price SF (2012) Ice-shelf basal channels in a coupled ice/ocean model. *Journal of Glaciology,* **58**(212), 1227–1244 (doi:10.3189/2012jog12j003)

Gourmelen N and others (2017) Channelized Melting Drives Thinning Under a Rapidly Melting Antarctic Ice Shelf. *Geophysical Research Letters,* **44**(19), 9796–9804 (doi:10.1002/2017gl074929)

Gudmundsson GH, Paolo FS, Adusumilli S and Fricker HA (2019) Instantaneous Antarctic ice sheet mass loss driven by thinning ice shelves. *Geophysical Research Letters,* **46**(23), 13903–13909 (doi:10.1029/2019gl085027)

Hillenbrand C-D and 14 others (2017) West Antarctic Ice Sheet retreat driven by Holocene warm water incursions. *Nature,* **547**(7661), 43–48, (doi:10.1038/nature22995)

Jacobs S and 6 others (2012) The Amundsen Sea and the Antarctic Ice Sheet. *Oceanography* 25(3), 154–163 (doi:10.5670/oceanog.2012.90)

Jenkins A, Nicholls KW and Corr HFJ (2010) Observation and Parameterization of Ablation at the Base of Ronne Ice Shelf, Antarctica. *Journal of Physical Oceanography,* **40**(10), 2298–2312 (doi:10.1175/2010jpo4317.1)

Jenkins A and 6 others (2010) Observations beneath Pine Island Glacier in West Antarctica and

implications for its retreat. *Nature Geoscience,* **3**(7), 468–472 (doi:10.1038/ngeo890)

Joughin I, Shapero D, Smith B, Dutrieux P, and Barham M (2021). Ice-shelf retreat drives recent Pine Island Glacier speedup. *Science Advances*, 7, eabg3080 (doi: 10.1126/sciadv.abg3080)

Kim S-Y and 8 others (2021) A 350-year multiproxy record of climate-driven environmental shifts in the Amundsen Sea Polynya, Antarctica. *Global and Planetary Change,* 205, 103589 (doi:10.1016/j.gloplacha.2021.103589)

Langley K and 8 others (2014) Complex network of channels beneath an Antarctic ice shelf. *Geophysical Research Letters,* **41**(4), 1209–1215 (doi:10.1002/2013gl058947)

Le Brocq AML and 10 others (2013) Evidence from ice shelves for channelized meltwater flow beneath the Antarctic Ice Sheet. *Nature Geoscience* **6**(11), 945–948 (doi:10.1038/ngeo1977)

Lee H and 8 others (2012) Continuously accelerating ice loss over Amundsen Sea catchment, West Antarctica, revealed by integrating altimetry and GRACE data. *Earth and Planetary Science Letters* 321, 74–80 (doi:10.1016/j.epsl.2011.12.040)

Macdonald GJ, Banwell AF, and MacAyeal DR (2018). Seasonal evolution of supraglacial lakes on a floating ice tongue, Petermann Glacier, Greenland. *Annals of Glaciology*, **59**(76pt1), 56–65 (doi.org/10.1017/aog.2018.9)

Mankoff KD, Jacobs S, Tulaczyk SM, and Stammerjohn SE (2012) The role of Pine Island Glacier ice shelf basal channels in deep-water upwelling, polynyas and ocean circulation in Pine Island Bay, Antarctica. *Annals of Glaciology*, **53**(60), 123-128 (doi: 0.3189/2012AoG60A062)

Marsh OJ and 6 others (2016) High basal melting forming a channel at the grounding line of Ross Ice Shelf, Antarctica. *Geophysical Research Letters,* **43**(1), 250–255 (doi:10.1002/2015gl066612)

Millgate T, Holland PR, Jenkins A and Johnson HL (2013) The effect of basal channels on oceanic ice-shelf melting. *Journal of Geophysical Research,* **118**(12), 6951–6964 (doi:10.1002/2013jc009402)

Morlighem M and 36 others (2020) Deep glacial troughs and stabilizing ridges unveiled beneath the margins of the Antarctic ice sheet. *Nature Geoscience* **13**(2), 132–137 (doi:10.1038/s41561-019-0510-8)

Mouginot J, Scheuchl B and Rignot E (2017) MEaSUREs Annual Antarctic Ice Velocity Maps, Version 1. *NASA National Snow and Ice Data Center Distributed Active Archive Center.*

Boulder, CO, USA (doi:10.5067/9t4epqxtjyw9)

Nakayama Y and 9 others (2019) Pathways of ocean heat towards Pine Island and Thwaites grounding lines. *Scientific Reports,* 9(1), 16649 (doi:10.1038/s41598-019-53190-6)

Nakayama Y, Menemenlis D, Zhang H, Schodlok M and Rignot E (2018) Origin of Circumpolar Deep Water intruding onto the Amundsen and Bellingshausen Sea continental shelves. *Nature Communications,* **9**(1), 3403 (doi:10.1038/s41467-018-05813-1)

Paolo FS, Fricker HA and Padman L (2015) Volume loss from Antarctic ice shelves is accelerating. *Science,* **348**(6232), 327–331 (doi:10.1126/science.aaa0940)

Pritchard HD, Ligtenberg SRM, Fricker HA, Vaughan DG, Broeke MR van den and Padman L (2012) Antarctic ice-sheet loss driven by basal melting of ice shelves. *Nature* 484(7395), 502–505 (doi:10.1038/nature10968)

Rignot E, Mouginot J and Scheuchl B (2017) MEaSUREs InSAR-Based Antarctica Ice Velocity Map, Version 2. *NASA National Snow and Ice Data Center Distributed Active Archive Center,* Boulder, CO, USA (doi:10.5067/d7gk8f5j8m8r)

Rignot E, Vaughan DG, Schmeltz M, Dupont T, and MacAyeal D (2002) Acceleration of Pine island and Thwaites glaciers, west Antarctica. *Annals of Glaciology*, 34, 189-194 (doi:10.3189/172756402781817950)

Rignot E and Steffen K (2008) Channelized bottom melting and stability of floating ice shelves. *Geophysical Research Letters,* **35**(2), L02503 (doi:10.1029/2007gl031765)

Scambos TA and others (2017) How much, how fast? A science review and outlook for research on the instability of Antarctica's Thwaites Glacier in the 21st century. *Global and Planetary Change* 153, 16–34 (doi:10.1016/j.gloplacha.2017.04.008)

Scambos TA, Haran TM, Fahnestock MA, Painter TH and Bohlander J (2007) MODIS-based Mosaic of Antarctica (MOA) data sets: Continent-wide surface morphology and snow grain size. *Remote Sensing of Environment,* **111**(2–3), 242–257, (doi:10.1016/j.rse.2006.12.020)

Sergienko OV (2013) Basal channels on ice shelves. *Journal of Geophysical Research,* **118**(3), 1342–1355 (doi:10.1002/jgrf.20105)

Smith B and 13 others (2020) Pervasive ice sheet mass loss reflects competing ocean and atmosphere processes. *Science* 368(6496), 1239–1242 (doi:10.1126/science.aaz5845)

Smith JA and 14 others (2017) Sub-ice-shelf sediments record history of twentieth-century retreat of Pine Island Glacier. *Nature,* **541**(7635), 77–80 (doi:10.1038/nature20136)

Steig E, Ding Q, Battisti D, and Jenkins A (2012) Tropical forcing of Circumpolar Deep Water Inflow and outlet glacier thinning in the Amundsen Sea Embayment, West Antarctica. *Annals of Glaciology, **53***(60), 19-28 (doi:10.3189/2012AoG60A110)

Stubblefield AG, Wearing MG, and Meyer CR (2023) Linear analysis of ice-shelf topography response to basal melting and freezing. *Proc. R. Soc. A*, 479, 20230290 (doi: 10.1098/rspa.2023.0290)

Wang S and 7 others (2023) Multidecadal pre- and post-collapse dynamics of the northern Larsen Ice Shelf. *Earth and Planetary Science Letters,* 609, 118077 (doi:10.1016/j.epsl.2023.118077)

Wearing MG, Stevens LA, Dutrieux P and Kingslake J (2021) Ice-Shelf Basal Melt Channels Stabilized by Secondary Flow. *Geophysical Research Letters,* **48**(21) (doi:10.1029/2021gl094872)

Wei W and 11 others (2020) Getz Ice Shelf melt enhanced by freshwater discharge from beneath the West Antarctic Ice Sheet. *The Cryosphere*, **14**(4) 1399-1408 (doi: 10.5194/tc-14-1399-2020)

Figure captions:

https://doi.org/10.1017/jog.2024.20 Published online by Cambridge University Press

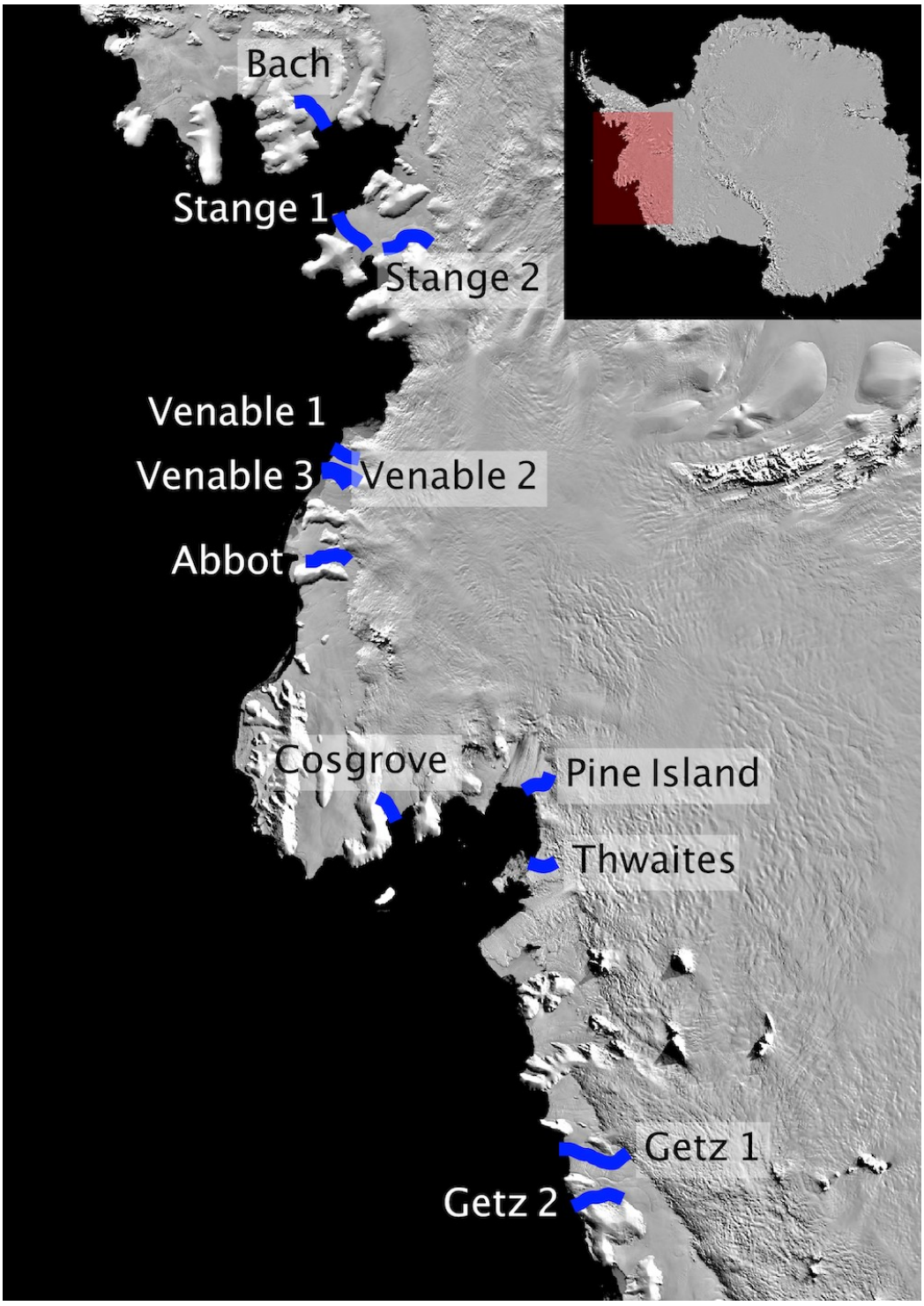

Figure 1: Basal channel locations in the ABS of West Antarctica. The 12 basal channels surveyed in this study are shown in blue. Background image is the MODIS Mosaic of Antarctica (MOA; Scambos and others, 2007).

https://doi.org/10.1017/jog.2024.20 Published online by Cambridge University Press

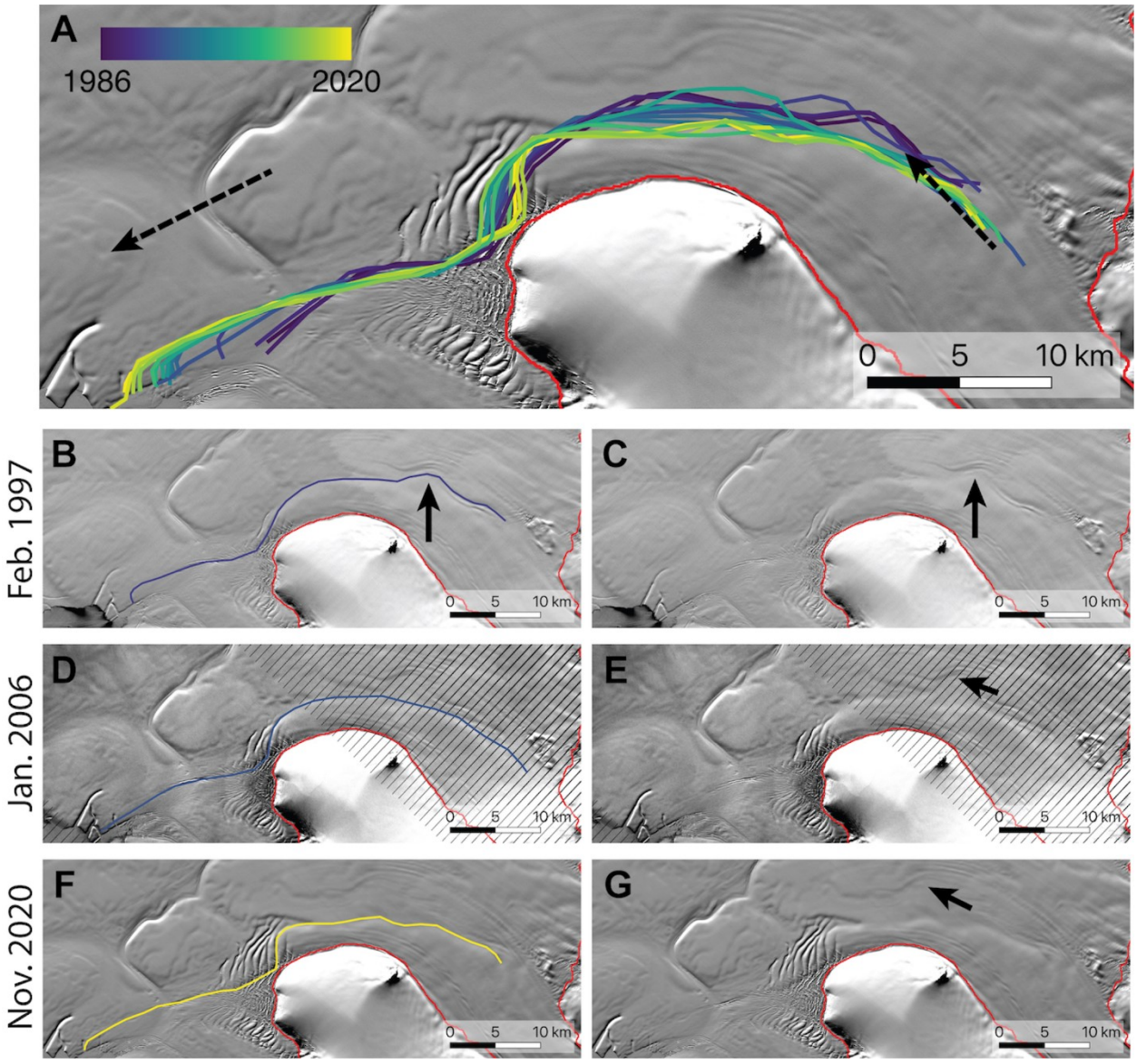

Figure 2: Stange 2 basal channel change. A. All channel traces for the Stange 2 channel from 1986-2020. Individual traces for 1997, 2006, and 2020 are shown in B-G, with the traced channel path displayed in the left-hand column (B, D, and F) and the same image without the path in the right-hand column (C, E, and G). Black dotted arrows in Panel A indicate approximate ice-surface velocity direction. Black arrows in panels B-C indicate a meander that is cut off from the channel in subsequent observations, and black arrows in panels E and G indicate this cutoff feature in later years.

https://doi.org/10.1017/jog.2024.20 Published online by Cambridge University Press

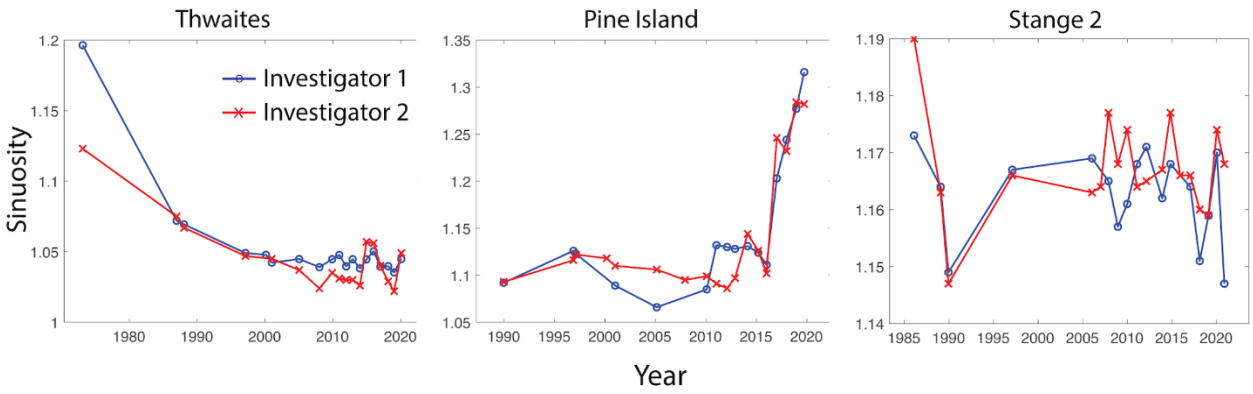

Figure 3: Sinuosity change. Observed sinuosity change for the channel evolution shown in Figures 2, 4, and 5. Thwaites experienced decreasing sinuosity, Pine Island experienced increasing sinuosity, and Stange 2 had no clear change in sinuosity through time. Results from independent digitizations by two investigators are shown in red and blue.

https://doi.org/10.1017/jog.2024.20 Published online by Cambridge University Press

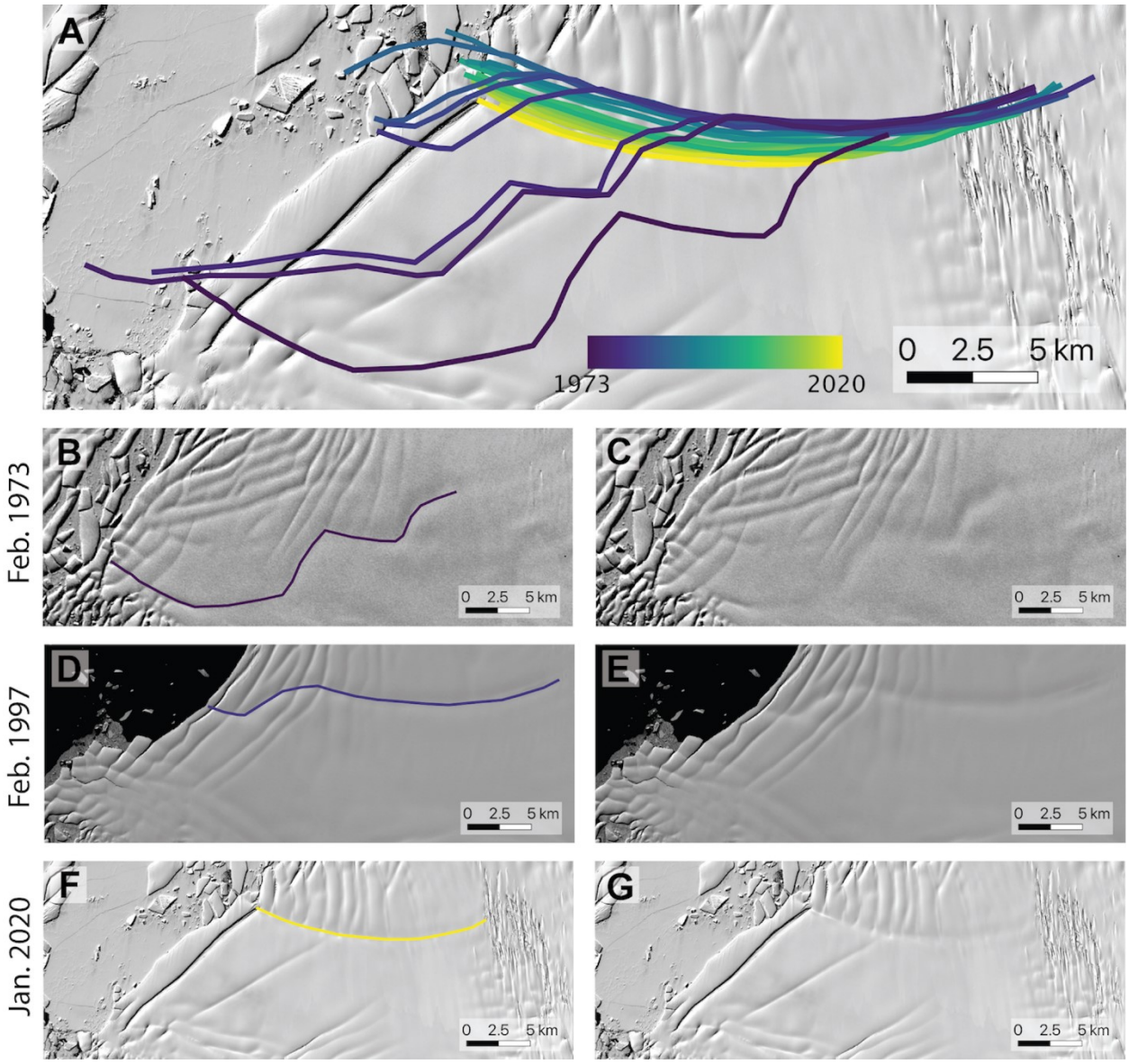

Figure 4: Thwaites basal channel change. A. All channel traces for the Thwaites channel from 1973-2020. Individual traces for 1973, 1997, and 2020 are shown in B-G, with the traced path displayed in the left-hand column (B, D, and F) and the same image without the path in the right-hand column (C, E, and G).

https://doi.org/10.1017/jog.2024.20 Published online by Cambridge University Press

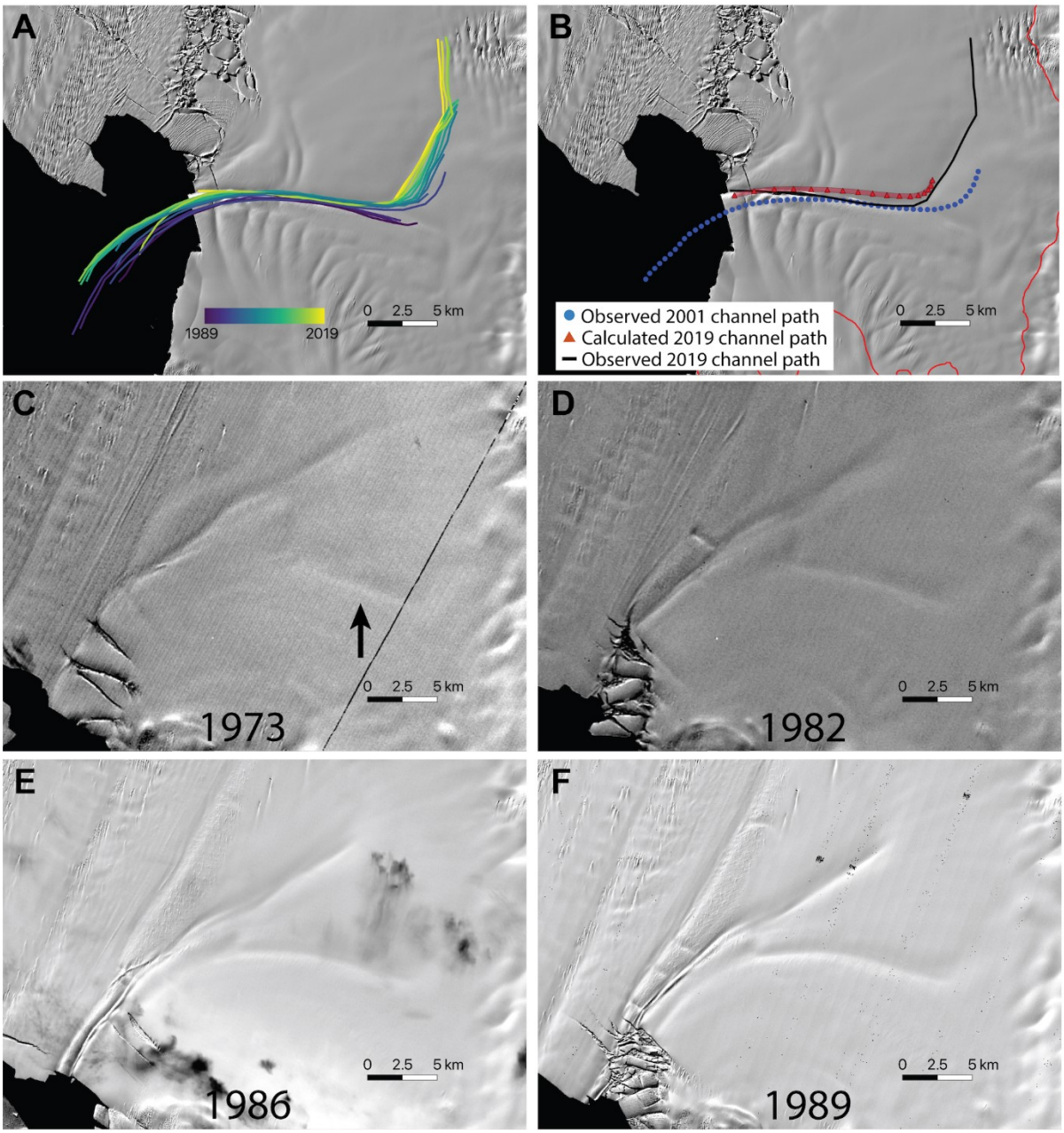

Figure 5: Evolution of the PIG basal channel. A. All digitized channel paths from 1989-2019. B. Predicted and observed locations of the basal channel in 2019. C-F. The initial growth of the channel, starting as a straight feature in 1973 (marked with an arrow, panel C) and evolving to a smoother path that reaches the ice edge by 1989 (panel F). Note that calving at the shear margin in the 1989 image (panel F) caused the ice-front to retreat to the mouth of the channel, so our digitizations began at this time.

https://doi.org/10.1017/jog.2024.20 Published online by Cambridge University Press

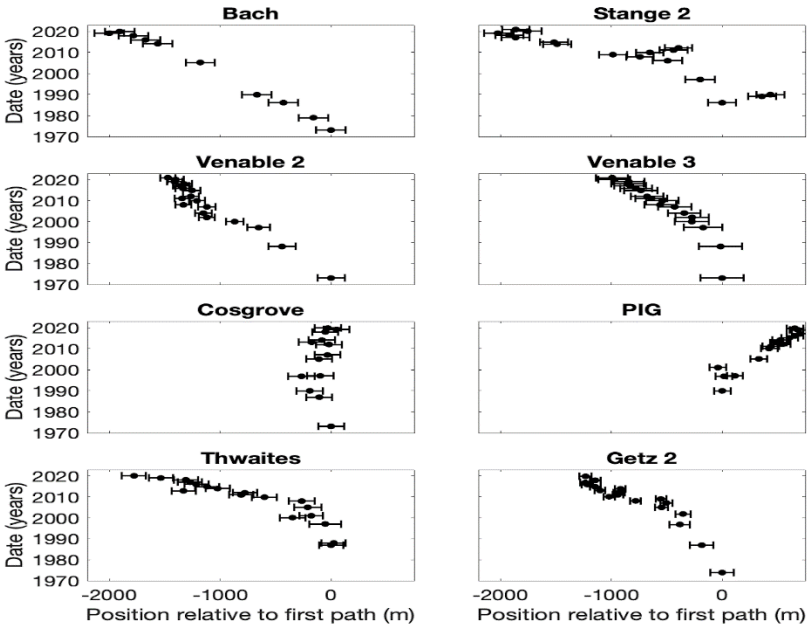

Figure 6: Locations of channel paths over time relative to the earliest digitized path. Locations of cross-lines where position measurements were taken are shown in Supplementary Fig. 1. Error bars for each channel location include digitization errors and the uncertainty associated with ice-flow rotation, as discussed in Methods.

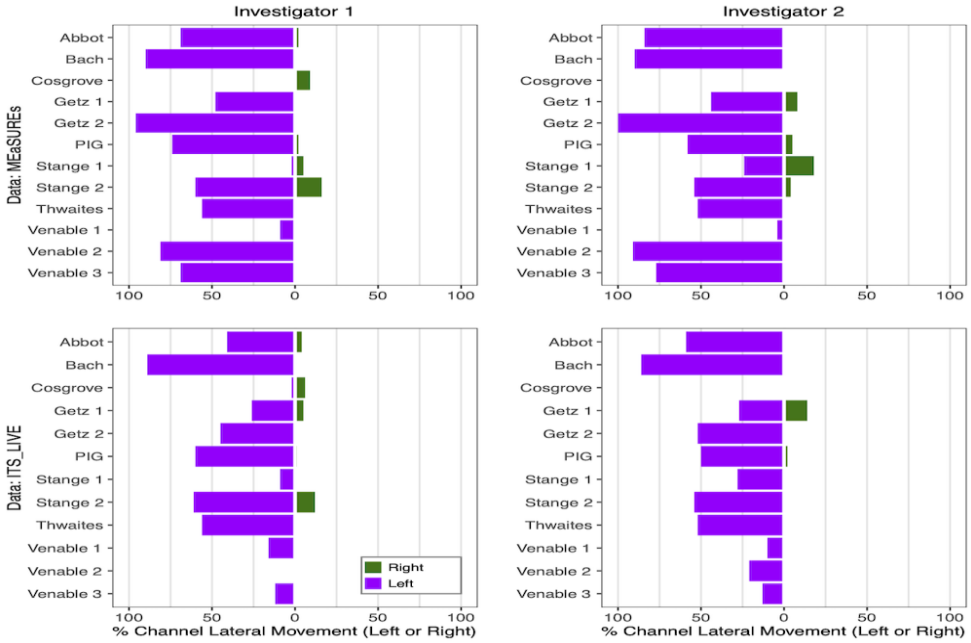

Figure 7: Flow-independent lateral channel migration. Colored bars show the percentage of each channel length that migrated significantly to the left (purple) or right (green) of its predicted location based on ice-surface velocity (Methods). Columns show the results based on two investigators independently tracing each channel, and rows show results produced with two

https://doi.org/10.1017/jog.2024.20 Published online by Cambridge University Press

published velocity fields: MEaSUREs (Rignot and others, 2017) and ITS_LIVE (Gardner and others, 2019).

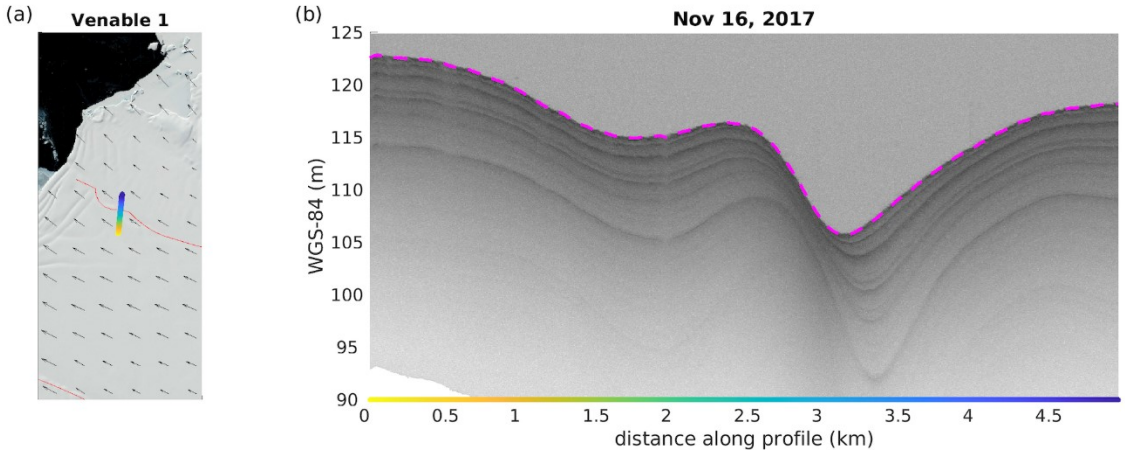

Figure 8: Airborne Snow radargram from Venable 1. Map in (a) shows the traced basal channel path in red, and arrows show surface velocity field from MEaSUREs. The location of an IceBridge snow radar transect, penetrating only the upper layers of the ice shelf, is shown in yellow-blue, with colors corresponding to distances on the x-axis in (b). Ice-shelf surface picks are in pink.

https://doi.org/10.1017/jog.2024.20 Published online by Cambridge University Press

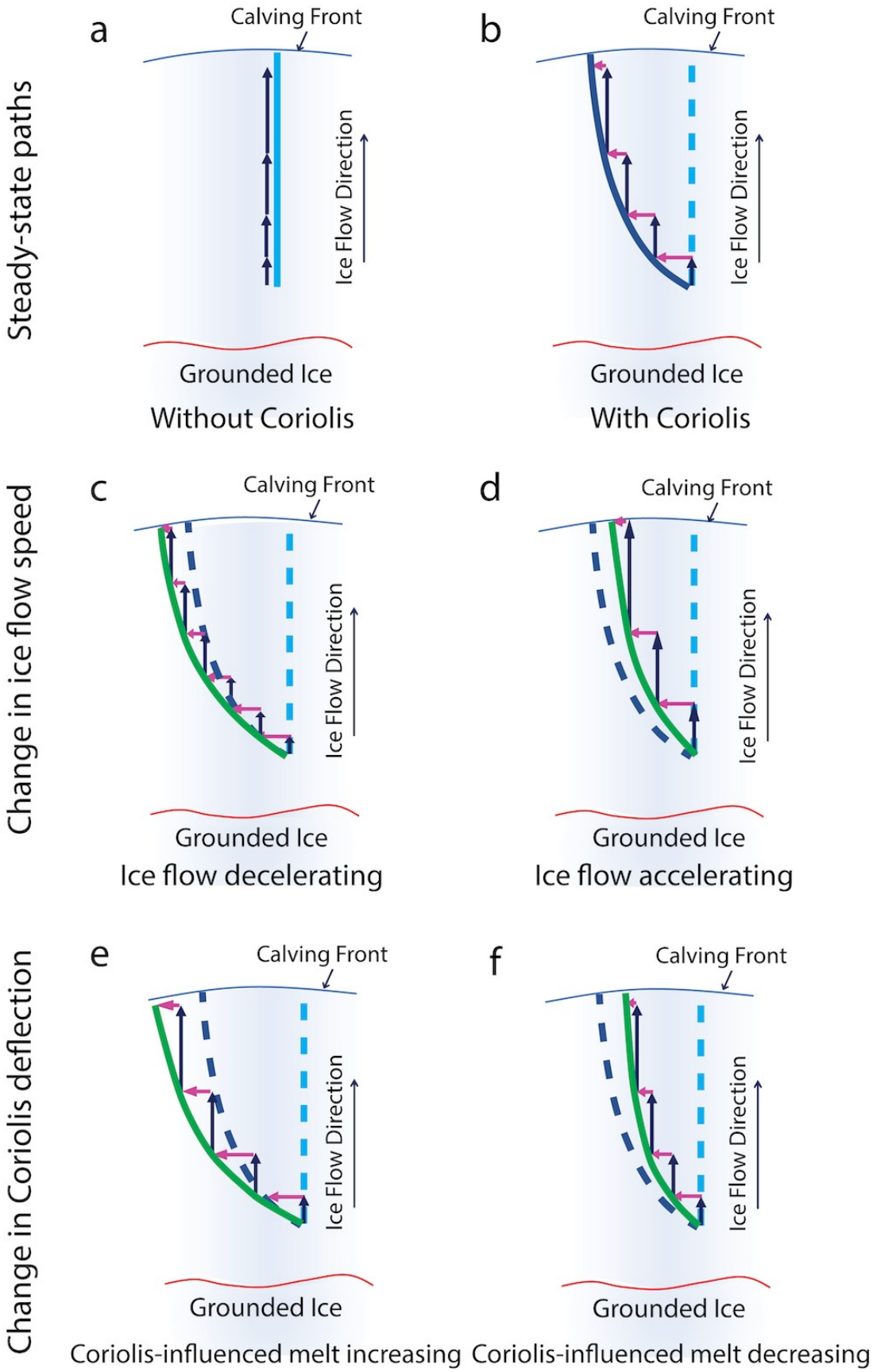

https://doi.org/10.1017/jog.2024.20 Published online by Cambridge University Press

Figure 9: Conceptual model of channel-path shape. Each panel shows an idealized ice shelf with a basal channel. Ice-flow vectors are shown as vertical black arrows, and Coriolis-influenced melt vectors are shown as horizontal magenta arrows. Note that Coriolis-influenced melt vectors are exaggerated so effects are visible. a) Idealized steady-state channel without Coriolis influence, shown as bold light blue line. Dotted light blue lines in panels b-f indicate the path of this no-Coriolis, steady-state channel for reference. b) Idealized steady-state channel with Coriolis influence, shown as bold dark blue line. Dotted dark blue lines in panels c-f indicate the path of this with-Coriolis, steady-state channel for reference. c-d) Non-steady channel paths under (c) decelerating ice flow (shorter black arrows), and (d) accelerating ice flow (longer black arrows). New channel paths are shown as bold green lines, which may represent either new steady states, or intermediate states during evolution to new steady states displaced even farther from the pre-perturbation steady states. e-f) Non-steady channel paths under (e) increased Coriolis-influenced melt (longer magenta arrows), and (f) decreased Coriolis-influenced melt (shorter magenta arrows). Again, new channel paths are shown as bold green lines, and may represent either new steady states, or intermediate states during further evolution.

https://doi.org/10.1017/jog.2024.20 Published online by Cambridge University Press